Journal Pre-proof

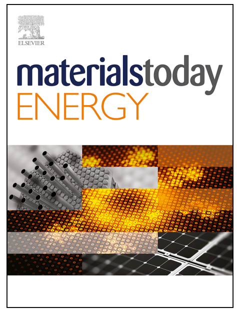

Engineering Redox Active Sites Enriched *3D-on-2D* Bimetallic Double Layered Hydroxide Electrode for Supercapatteries

Pugalenthiyar Thondaiman, Chellan Justin Raj, Rajavel Velayutham, Antonysamy Dennyson Savariraj, Ramu Manikandan, Voz Cristobal, Byung Chul Kim

PII: S2468-6069(22)00240-4

DOI: https://doi.org/10.1016/j.mtener.2022.101182

Reference: MTENER 101182

To appear in: *Materials Today Energy*

Received Date: 28 July 2022

Revised Date: 13 October 2022

Accepted Date: 14 October 2022

Please cite this article as: P. Thondaiman, C.J. Raj, R. Velayutham, A.D. Savariraj, R. Manikandan, V. Cristobal, B.C. Kim, Engineering Redox Active Sites Enriched *3D-on-2D* Bimetallic Double Layered Hydroxide Electrode for Supercapatteries, *Materials Today Energy*, https://doi.org/10.1016/j.mtener.2022.101182.

CRediT authorship contribution statement

Pugalenthiyar Thondaiman: Conceptualization, Methodology, Validation, Formal analysis, Investigation, Writing - original draft, Writing - review & editing. **Chellan Justin Raj:** Supervision, Methodology, Investigation, Validation, Writing - Review & Editing. **Rajavel Velayutham:** Formal analysis, Investigation, Validation. **A. Dennyson Savariraj:** Investigation, Validation, Writing - Review & Editing. **Ramu Manikandan:** Investigation, Writing - review & editing, Validation, Visualization Validation. **Voz Cristobal:** Formal analysis, Investigation, Writing - review & editing. **Byung Chul Kim:** Conceptualization, Supervision, Methodology, Validation, Investigation, Resources, Writing - review & editing, Visualization, Project administration, Funding acquisition.

Graphical Abstract

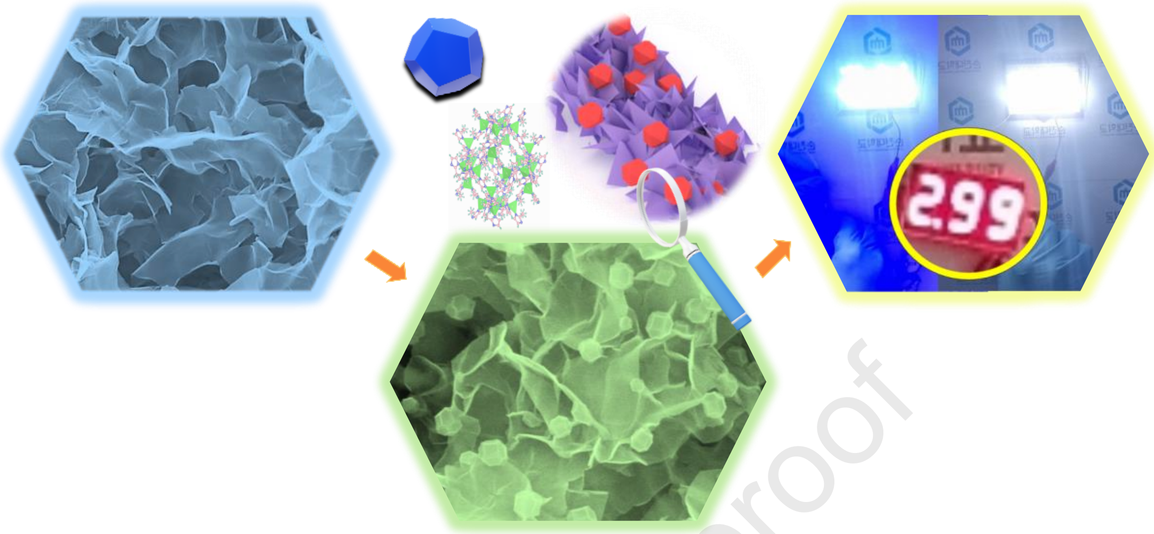

Engineering Redox Active Sites Enriched *3D-on-2D* Bimetallic Double Layered Hydroxide Electrode for Supercapatteries

Pugalenthiyar Thondaiman[a], Chellan Justin Raj[b], Rajavel Velayutham[a], Antonysamy Dennyson Savariraj[a], Ramu Manikandan[c], Voz Cristobal[d], Byung Chul Kim[a]*

[a] Department of Advanced Components and Materials Engineering, Sunchon National University, Suncheon-si, Republic of Korea

[b] Physics Division, School of Advanced Sciences, Vellore Institute of Technology (VIT), Chennai Campus, Tamil Nadu, India

[c] Department of Fiber System Engineering, Yeungnam University, Gyeongsan, South Korea

[d] Department d'Enginyeria Electrònica, Universitat Politècnica de Catalunya, Barcelona, Spain

* *Corresponding author*

Abstract

The functionalization of structural nanoengineered battery-type electrodes has aided the emergence of supercapattery (SCp) subclass, which enables a wide range of applications. Herein, our research work provides a platform for two-step fabrication of nanoengineered *3D-on-2D* structure as a promising approach to obtain high performance battery-type electrodes. The hierarchical 2D NiCo bimetallic LDH NC(12)40 electrode was fabricated using electrodeposition, while the nanoengineered 3D ZIF-67 on 2D LDH electrode was achieved via pseudomorphic replication techniques. The fabricated *3D-on-2D* NC(12)40-30 electrode reveals a maximum areal capacity of 1044 mC cm^{-2} at a current density of 4 mA cm^{-2} in 6 M KOH electrolyte. Furthermore, NC(12)40-30//AC was integrated as a SCp device, achieving a maximum specific capacitance of 63 F g^{-1} and maximum specific energy and power of 20.5 W h kg^{-1} and 8522.7 W kg^{-1}, respectively, with improved capacitance retention (85 %) even after 10,000 cycles. Thus, the assembled SCp coin cell displays 18-LED illumination in four different commercial LED colors, indicating the viability of the battery-type electrode for SCp development.

Keywords: *3D-on-2D*, Bimetallic LDH electrode, NiCo-LDH, ZIF-67, Electrodeposition, Pseudomorphic replication, Supercapattery.

1. Introduction

Supercapacitors (SCs) research has created a great deal of interest in developing the foundation for energy storage technology with fast charging and high power with super long-life cycles. This tends to result in the smooth implementation of regenerative braking systems for electric vehicles, heavy duty vehicles, and light rail [1]. However, SCs still provide a limited range of energy density, making it intricate to emphasis on expanding to other applications. In fact, in the mid-1990s, Hybrid Supercapacitors (HSC) was proposed as a combination of capacitive-type and battery-type electrodes for the development of new electrochemical storage devices [2]. The excellent HSC systems have unique characteristics that are achieved by using crystalline or hybrid nanostructured electrodes with divergent or synergistic energy storage mechanisms. According to recent research, HSC class is recognized to be the best potential candidate to achieve high-performance energy storage system [3]. Supercapattery (supercapacitor + battery) approach has been coined to represent a typical categorization of HSC frameworks that allows for the integration of a capacitor-type electrode (as the power source via an electric double-layer approach) and a battery-type electrode (as the energy origin via Faradaic process) [4,5]. Carbon-based materials have been used in capacitor-type electrodes resulting in a rapid response, high accessibility of electrolyte ions, and enhanced energy storage capacity due to the double capacitor layer effect [6,7]. The selection of battery-type electrode materials with nanostructure is predominantly composed from transition metal-based substances, such as transition metal derivatives (TMX; X = oxides, hydroxides, sulfides, phosphides) and transition metal-based organic frameworks (MOFs) [2,8,9]. Transition metal hydroxides (TMOHs) stand out as a good alternative for enhanced capacitance by tailoring its electrochemical performance among various battery-type materials. Among the various morphological strategies, 3D-on-2D structural engineering provides a larger active surface area and high structural integrity, leading to a better ion transport path in electrochemical behavior. Typically, TMOHs based layered double hydroxides (LDHs) are a class of two-dimensional (2D) layered family that can be represented as, $[M^{2+}_{1-x} M^{3+}_{x} (OH)^{2}]_{x}^{+}(A^{n-})_{x/n} \cdot mH_2O$. The architecture of 2D bimetallic LDH is mainly composed of cationic charged brucite-like host layers (M^{2+}: divalent and M^{3+}: trivalent metal cations) with traceable charge-balancing interlayer anions (A^{n-}) [8,10]. In recent years, 2D LDH chemistry has gained great interest due to its high theoretical specific capacitance and abundant electrochemical active site in the field of energy storage [10–14]. Besides, 2D bimetallic NiCo LDH claims to be an ideal battery-type electrode material for SCp, and notable research has discovered that structural engineering of nanomaterials could further boost electrochemical kinetics in SCp. It would be beneficial to further explore the 3D-on-2D hierarchical structure, which revealed an effective interaction between faradaic sites of energy storage and electroactive species during the charge/discharge process [13–15].

Considering these variances, herein, this work we focused on the fabrication of a nanoengineered *3D-on-2D* hierarchical structure to be used as a battery-type electrode in supercapattery. The nano-architecture of *3D-on-2D* electrode was fabricated in a two-step process using a simple and low-cost strategy. Primarily, cathodic electrodeposition (CED) methodology was used to achieve 2D bimetallic NiCo LDH on Ni foam, an effective and reliable method for constructing 2D structured hydroxides. The CED process explored various electrodeposition bimetallic ratios and electrodeposition times to obtain excellent 2D NiCo LDH compositions. Lastly, the appropriate 2D NiCo LDH compositions were subjected to the pseudomorphic replication technique in order to fabricate a *3D-on-2D* hierarchical architecture electrode material. After fabrication, the electrodes were carefully examined using structural characteristics and electrochemical performances properly. Moreover, for supercapattery device studies, an optimized hierarchical *3D-on-2D* electrode (battery-type) and activated carbon (EDLC-type) were used as positive and negative electrodes, respectively.

Similarly, the supercapattery was designed and constructed in a coin-cell for real-time evaluation. From the detailed analysis, hierarchical *3D-on-2D* bimetallic NiCo LDH electrode revealed outstanding electrochemical performance and proved as an effective electrode for energy storage applications.

2. Experiment Section

Preparation of 2D bimetallic template: A 2D structured Ni-Co bimetallic template on Ni foam was obtained by potentiostatic electrodeposition (ED) with some modifications in previously report [16,17]. Prior to electrodeposition, the Ni foam working electrode was pre-cleaned with 10 % HCl, DI water (until residues reached pH 7), and acetone, while standard Ag/AgCl and Pt wires were used as reference and counter electrodes, respectively. The deposition solution was prepared in 20 ml of an aqueous mixture of 25 mM Ni precursors, 50 mM Co precursors (1:2 molar ratio) and 150 mM urea. In the three-electrode system, electrodeposition was conducted at a constant potential of -1.0 V for 40 min. After deposition, the electrode was gently washed with DI and dried in a hot air oven for 12 h at 65 °C, the NC(12)40 template with green color was obtained and stored until further use. To perform the concentration dependent experiments, 1:1 and 2:1 molar ratio of Ni and Co precursors were studied at constant ED time (40min). These bimetallic electrodes have been denoted as NC(11)40 and NC(21)40, respectively. For the time-dependent experiments, samples with 30- and 50-min ED times were prepared in 1:2 ratio of Ni and Co. These samples have been designated as NC(12)30 and NC(12)50, respectively. The resulting mass of deposited electroactive material reached ~ 6 mg.

Preparation of 3D-on-2D surface treatment: A simple 3D surface treatment was performed by using a pseudomorphic replication approach. In a typical procedure, the NC(12)40 electrode was immersed vertically in 10 mL mixture of DI/methanol (2:3), with 2.05 g of 2-

methylimidazole dissolved for periods of 15, 30 and 45 min, and maintained at room temperature and the resulting electrodes were labeled as NC(12)40-15, NC(12)40-30 and NC(12)40-45 samples, respectively. Lastly, the electrodes were washed with DI water gently and dried for 12 h in a hot air oven at 65 °C and stored until further use. The description of chemicals and reagents, physicochemical characterization, electrochemical measurements, and the fabrication of supercapattery (SCp) are presented in the supporting information of the manuscript.

3. Results and Discussion

A schematic diagram of the two-step fabrication of nanoengineered *3D-on-2D* hierarchical battery-type electrodes for a supercapattery application, is illustrated in Fig. 1. The current collector is the central component of the energy storage system, serving as the electrical connection between both electroactive materials and electronic terminals. For this, nickel (Ni) foam is used as an ideal current collector (electrode material) because of its porous structure, large surface area, and good electrochemical conductivity. Prior to electrodeposition, the Ni foam is acid cleaned on the surfaces to remove contaminants such as oil, grease, and dust that may affect the performance of such electrodes. Initially, a cathodic electrodeposition (CED) approach is being used, and the deposition solvent is a mixture of nickel(II) nitrate, cobalt(II) nitrate, and urea in an aqueous (DI) medium. The selection of urea was mainly owning to its influence to promote leveling effect by urea molecules that plays a significant role as a growth directing agent, which facilitates the uniform orientation of the crystalline nature. The resulting 2D bimetallic Ni(1)Co(2) composition with 40 min of electrodeposition LDH electrode was proposed using CED method as an effective and reliable battery-type electrode for subsequent studies. The reactions that occur when an electric current passes through the electrolyte during the electrodeposition are as follows (1) and (2), [18]

$$NO_3^- + 7H_2O + 8e^- \rightarrow NH_4^+ + 10OH^- \quad (1)$$

$$M^{n+} + n(OH)^- \rightarrow M(OH)_n \quad (2)$$

The reduction of NO_3^- and subsequent transformation of OH^- anions from nitrate ions during cathodic electrodeposition has been presented in equation (1). The reaction (2) states that under deposition conditions, the cathodic reduction of the required proportions of M^{n+} (M is Co^{2+} and Ni^{2+} metal ions) in nitrate baths with the hydroxyl that allowing the formation of bimetallic NiCo LDH to precipitate in Ni foam sites [19–21]. Finally, a pseudomorphic replication strategy was utilized for *3D-on-2D* hierarchical architecture of battery-type electrodes. The pseudomorphic replication phenomenon derives from the concept of mineralogy and entails the transformation of an existing parent phase into a new thermodynamically stable phase using interface-coupled and dissolution-precipitation mechanisms for nucleation and crystallization [22,23]. By using this phenomena, 3D sodalite framework of ZIF-67 was constructed by bridging with 2-methylimidazole (MeIm) ligands in the solution and counteracting the surface Co ions in the forest 2D LDH structure [24,25]. In this study, a 2D bimetallic NC(12)40 LDH electrode was immersed in a solution containing MeIm in a mixture of DI/methanol with the ratio 40:60, at different immersion times (15, 30, and 45 minutes) were examined. These are referred as NC(12)40-15, NC(12)40-30, and NC(12)40-45 samples, respectively. The structural and electrochemical characterizations of the fabricated electrodes were investigated in detail below.

3.1 Material Characterizations

The structural interpretation of *3D-on-2D* bimetallic LDH is confirmed by X-ray diffraction (XRD) patterns shown in Fig. 2(a). The XRD spectra of NC(11)40 (brown), NC(21)40 (green), NC(12)40 (violet) and NC(12)40-30 (red) exhibits a pattern (003), (006), (009), and (110) facets which can be identified to rhombohedral phase of hydrotalcite LDH family (JCPDS Card no. 14-0191). Additional peaks can be seen in NC(12)40 and NC(21)40, which are reflections of $Co(OH)_2$ phase (JCPDS#30-0443) and $Ni(OH)_2$ phase (JCPDS#14-0117), respectively [26,27]. The corresponding XRD pattern of NC(12)40-30 XRD possesses significant major peaks at (110), (200), (211), and (222) pattern as well as some minor peaks, in response to a single crystal plane of ZIF-67 that matched identically with an earlier report [28]. It is unambiguous evidence that the crystalline phase of ZIF-67 framework has been constructed with a bimetallic LDH electrode. Moreover, the three profound peaks were observed due to the nickel foam substrate [29]. In order to peruse the information of energy states and chemical composition, X-ray photoelectron spectroscopy (XPS) was carried out for NC(12)40 and NC(12)40-30 electrodes, and XPS data could be fitted by Gaussian and Shirley background using Origin software. The survey scan spectra are exhibited in Fig. 2(b), which confirms the presence of elements such Co, Ni, O, C and N in NC(12)40-30 and Co, Ni and O elements in the NC(12)40 electrodes, respectively. The presence of C 1s and N 1s in NC(12)40-30 demonstrated that 3D ZIF-67 was effectively integrated into the 2D bimetallic LDH electrodes, as evidenced in the survey spectra. Moreover, C1s and N1s observed through 3D ZIF-67, implying the ZIF-67 pseudomorphic growth approach achieved by using O-H ions from LDH surface coordination [23,25]. Presumably, it is worth noting that the successful hierarchical unit cell structure of 3D ZIF-67 with 2D bimetallic LDH is illustrated in Fig. 2(c). The description of high-resolution XPS spectra are produced in the supporting information of the manuscript. Evidently, the obtained XRD and XPS analysis provides the validation of 2D bimetallic LDH and affirms the formation of ZIF-67 on 2D structured electrode.

Regarding morphological analysis, the prepared samples were observed using field emission scanning electron microscopy (FE-SEM) with energy dispersive X-ray spectroscopy (EDX) and high-resolution transmission electron microscopy (HR-TEM), as shown in Fig. 3 and Fig. S(1-5). The morphological studies of different bimetallic ratio of electrodes and EDX analysis of *3D-on-2D* electrodes are presented in the supporting information of the manuscript. As a result, the NC(12)40 LDH revealed a forest of 2D sheets with excellent permeability structure, which has immense opportunities to be implemented for superior *3D-on-2D* architecture towards effective supercapacitor performance. Furthermore, the low magnifications of the FE-SEM morphology of *3D-on-2D* grafted electrodes NC(12)40-15, NC(12)40-30, and NC(12)40-45 can be seen in Fig. S3(a-c), respectively. The phenomenon of *3D-on-2D* hierarchical structure could be interpreted by active Co-ions sites performing as an architecture-directing agent, contributing to the Ostwald nucleation for the formation of 3D rhombic dodecahedron structure of ZIF-67 on the surface of 2D bimetallic LDH [34]. The FE-SEM images of NC(12)40-15 obtained revealed that very few 3D ZIF-67 grown over the 2D layered structure was indeed recognizable at higher magnifications (Fig. 3(a)) [9,17,35,36]. In the meantime, the *3D-on-2D* hierarchical structure of NC(12)40-30 depicts a growth mechanism of ZIF-67 uniformly distributed 3D rhombic dodecahedron structure over the 2D LDH (Fig. 3(b)). This indicated that 3D ZIF-67 has been effectively grown on the 2D bimetallic LDH surface without dispute, suggesting more electrochemical active regions with significantly improved electron mass transfer performance [34]. However, NC(12)40-45 (Fig. 3(c)) indicate an irregular 3D ZIF-67 structure growth on the 2D layered structure, influencing the inadequate ion transfer permeability to interact with the bimetallic LDH layered. Likewise, in Fig. 3(d), presenting high resolution transmission electron microscopy (HRTEM) and selected area electron diffraction (SAED) were also carried out for the NC(12)40-30 to further discuss its reliability of the crystalline nature. It is clearly evident that the hexagonal structure is revealed from the low magnification of the TEM images shown in Fig. 3d(i), confirming the stacked 2D LDH structure of previous reports [37]. Note that Fig. 3d(ii) is a magnified expression of the blue region in Fig. 3d(i), where 2D bimetallic LDH and 3D ZIF-67 symbolizes in the respective yellow and pink regions. In this regard, using the

GATAN Microscopy Suite (GMS) software, the micrographs of HRTEM images could be further evaluated to generate the fast-Fourier transforms (FFTs) and inverse FFTs (IFFT) patterns, and line profile for analyzing the crystalline attributes (Fig. S5). Using GMS software, the high-crystalline 2D LDH structure is displayed in the insert of Fig. 3d(iii), and the corresponding FFT and IFFT patterns are shown in Fig. 3d(v and vi). The applied mask area (insert of Fig. 3d(vi)) of selected yellow spots implies the IFFT pattern and represents the line profile (Fig. S4(a)) which recorded the inter-planar d-spacing of 0.351 nm that matches to the indexed with (0 0 6) crystal plane of bimetallic LDH resolved in XRD spectra [38]. Similarly, the applied mask area (insert of Fig. 3d(ix)) of selected pink spots indicates the IFFT pattern and corresponding line profile (Fig. S4(b)) with d-spacing of 0.79 nm that can be indexed to the (2 0 0) crystal plane of ZIF-67 and also well matches XRD spectra [34]. As shown in Fig. 3d(vii) and Fig. 3d(x) the SAED pattern of 2D LDH structure and 3D ZIF-67 revealed polycrystalline and high crystalline properties of *3D-on-2D* hierarchical bimetallic electrodes, respectively [39]. Thus, the HRTEM with SAED and GMS analysis confirmed the formation of *3D-on-2D* hierarchical ZIF-67 with high crystallinity.

3.2 Electrochemical characterizations

The description of different ratio (Ni, Co precursors of 1:1, 2:1 and 1:2) of bimetallic LDH electrodes and electrodeposition times (30, 40, and 50 min) for NC(12)40 are presented in the supporting information of the manuscript. The overall charge/discharge performance of the 2D bimetallic NC(12)40 electrode demonstrated excellent higher areal capacity of 661 mC cm^{-2} as compared to other 2D counterparts which represents the characteristic features of fast non-capacitive faradaic battery-type electrode materials. This behavior could be a 2D interlayer of active sites due to the increased proportion of Co in this bimetallic composition [40]. It can be seen that the high $Co^{2+}/^{3+}$ content caused the emergence of the conducting

CoOOH during the discharge process and excellent permeable network seen in FESEM (Fig. S1) which induces superior OH^- diffusion on the surface and better redox kinetics.

Electrochemical performance of 3D-on-2D bimetallic LDH architecture: The *3D-on-2D* structural nano-engineering of NC(12)40 bimetallic electrode reviewed systematically in electrochemical characterizations to witness a promising strategy in energy storage applications. For this, a set of electrochemical studies were conducted to the distinctive hierarchical structure of NC(12)40-15, NC(12)40-30 and NC(12)40-45 electrodes. The charge storage characteristics of the prepared electrodes were analyzed by electrochemical properties such as cyclic voltammetry (CV), Galvanostatic charge/discharge (GCD) and electrochemical impedance spectroscopy (EIS) in 6 M KOH solution using a three-electrode system. The relative CV plots for NC(12)40, NC(12)40-15, NC(12)40-30 and NC(12)40-45 electrodes were measured at a constant scan rate of 4 mV s^{-1} with a potential window in the range of -0.2 V to +0.5 V, as displayed in Fig. 4(a). The broad CV profiles has been influenced by the performance of higher redox reactions enabled in *3D-on-2D* structure, stating that 3D ZIF-67 effectively contributes to higher faradaic charge storage compared to the 2D battery-type NC(12)40 bimetallic electrode. Interestingly, NC(12)40-30 depicts an outstanding electrochemical activity in relation to other configurations, proposing that uniform growth of 3D ZIF-67 rhombic dodecahedral hierarchical structure on 2D LDH enriches more accessible of OH^- ions, leading to highly reversible battery like faradaic reactions [34,41]. The CVs of different *3D-on-2D* hierarchical structure electrodes were measured with different scan rates (2, 4, 8, 12, 16, and 20 mV s^{-1}) (Fig. S8(a-c)). The CV plots of NC(12)40-30 presented (Fig. S8(b)) exhibited perfectly maintained without deformation of enclosed area and high reversibility with less polarization than their counterparts. It is worth noting that the charge storage achieved through the CV area indicated a synergistic performance of both the 3D ZIF-67 (diffusion controlled) and the faradic processes of the 2D bimetallic LDH structure (non-capacitive behavior). From these observations, the synergism of 3D ZIF-67 on 2D bimetallic LDH structure provide more surface electroactive sites cause a rapid electron-ion transfer at the electrode material. For further investigation of charge/discharge studies, GCD profiles of different *3D-on-2D* hierarchical structure electrodes were conducted at a constant current density of 4 mA cm^{-2} with a potential window in the range of -0.2 V to +0.5 V, as displayed in Fig. 4(b). The GCD profiles of *3D-on-2D* hierarchical NC(12)40-15, NC(12)40-45 and NC(12)40-30 electrodes are exhibited in Fig. S8(d-f), respectively. It would be evident from the GCD curves that a quasi-symmetrical profile can be described to the distinct battery-type performance noted from the redox reaction pertaining to the CV profile (Fig. 4(a)). In Fig. 4(c), the areal capacities were determined from the GCD profiles of NC(12)40, NC(12)40-15, NC(12)40-30, and NC(12)40-45 electrodes using equation (1) in supporting information. The calculated values were 661, 814, 1044, and 927 mC cm^{-2} at the current density of 4 mA cm^{-2}, respectively. It has been established that the higher areal capacity of the NC(12)40-30 electrode due to the high permeability of the *3D-on-2D* hierarchical structure can contribute to improved charge accumulation and OH^- penetration during charge/discharge pathways. This is demonstrated by the fact that the battery-type NC(12)40-30 provided more electroactive sites from 2D LDH, resulting in charge storage via faradaic reaction, as well as rapid electro-adsorption/desorption facilitated by 3D ZIF-67, resulting in non-capacitive charge storage behavior. Additionally, the rate capabilities (Fig. S8(g)) of prepared *3D-on-2D* electrodes significantly reduced at higher current densities that restricted the electrochemical behavior. Besides that, long-term cycle stability of *3D-on-2D* hierarchical structure of NC(12)40-30 electrode achieved using GCD technique at constant current density of 15 mA cm^{-2} for 5,000 cycles is shown in Fig. 4(d). At the 5000th cycle, the NC(12)40-30 electrode retains approximately 80% areal capacity observed in its 1st cycle, demonstrating remarkable electrochemical stability with adequate reversibility. In addition to that, electrochemical impedance spectroscopy (EIS) was used to examine the electrochemical interfacial behavior of the *3D-on-2D* hierarchical structure of NC(12)40-15, NC(12)40-30, and NC(12)40-45 electrodes. From the Nyquist plot of EIS analysis (Fig. 4(e)), NC(12)40-45 exhibits outstanding electrochemical performance compared to its counterparts interpreted with equivalent circuit and the values obtained are detailed in Table S1 and Fig. S6 (l). The significantly increased EIS values compared to NC(12)40 electrodes are attributed to the formation of 3D ZIF-67. The evidenced of NC(12)40-30 electrode to be nearly similar with slight improvement of R_s and W_R with roughly comparable R_{ct} to the other samples, which was appropriate modeling to the prospect of OH^- mass transfer at electrode/electrolyte interface of charge transfer functionalities [42,43]. The post-mortem investigation was conducted by interpreting the FE-SEM images of the *3D-on-2D* nanoengineered electrode to examine the morphological behavior changes after the cycling test. The micrographs of the NC(12)40-30 electrode before and after electrochemical cycling are shown in Fig. S9, and the morphology revealed slight variations on the surface, but it remains intact after long cycling. This demonstrates that even after 5000 GCD cycles, the electrode sustains excellent stability in 6 M KOH electrolyte. Thus, a nanoengineered *3D-on-2D* architecture of NC(12)40-30 bimetallic battery-type electrode demonstrates excellent electrochemical behavior with extended features due to its high active Co sites, which are subjected to boosting capacity enhancement in supercapacitor applications.

Electrochemical characterizations of supercapattery: Typically, the electrochemical behavior of the positive and negative electrodes was evaluated using a three-electrode system. The commercial activated carbon (AC) was preferred as the negative electrode material, and electrochemical characterization and SCp device configuration are discussed in the supporting information. To perform device analysis, the series of CV (Fig. 5(c)) and GCD

(Fig. S10(e)) studies were conducted at 50 mV s^{-1} and 4 A g^{-1} with various voltage windows (1.2, 1.4, 1.5, and 1.6 V), respectively. The SCp device revealed that the operating cell voltage can be limited up to 1.5 V without polarization in the CV, and the GCD profiles further endorse the CV curve with excellent capacitance delivery. Thus, the electrochemical tests are performed on the assembled SCp device (NC(12)40-30/AC) in the voltage window range of 0 to 1.5 V in 6 M KOH. The different CV scan rates (10, 25, 50, 75, and 100 mV s^{-1}) of NC(12)40-30//AC are depicted in Fig. 5(d), which shows a quasi-rectangular curve with a broad battery-like with EDLC performance and better reversibility. At slow scan rates, the charging/discharging of OH^- ions is constructively encountered on the structurally engineered *3D-on-2D* positive NC(12)40-30 electrode, which acts as a battery type supercapacitor, and the K^+ ions are absorbed/desorbed on the negative AC electrode surface, which acts as typical EDLC behavior. It should be noted that the degree of distortion of CV profiles at higher scan rates changes from reversible to quasi-reversible, mainly due to the interaction of ions on the electrode surface. The GCD profiles of the NC(12)40-30/AC device (Fig. 5(e)) were carried out for various specific currents (1, 2, 3, 4, 5, 6, 8, and 10, 12 A g^{-1}) and showed the stable near symmetrical characteristics, clearly stating sustainable charge storage performance due to its inherent reversible electrochemical reactions. The specific capacitance (F g^{-1}) was estimated from GCD using equation (2) in supporting information, and the maximum capacitance of SCp was found to be 63, 59, 55, 50, 47, 43, 38, 34, and 30 F g^{-1} for specific currents of 1, 2, 3, 4, 5, 6, 8, 10, and 12 A g^{-1}, respectively as shown in Fig. 5(f). Moreover, the performance of SCp was evaluated by specific energy (E_s) and specific power (P_s) using equation (4) and (5) in supporting information and illustrated as Ragone plot shown in Fig. 5(g). The NC(12)40-30/AC device demonstrated an outstanding E_s of 20.5 W h Kg^{-1} for a P_s of 774.5 W Kg^{-1} at 1 A g^{-1} and considerably retained 9.01 W h Kg^{-1} for a maximum P_s of 8522.7 W Kg^{-1} at 12 A g^{-1}. The resulting values of E_s and P_s summarize the proper sustainable charge storage mechanism of SCp and are significant compared to recent reports, as shown in Table S2. Furthermore, Fig. 5(h) demonstrates the long-term cycle stability of the NC(12)40-30/AC device achieved using GCD technique at constant 6 A g^{-1} for 10,000 cycles. The specific capacitance of the SCp device at the 10,000th cycles retains about ~ 85 % of its 1st cycle, evidencing an excellent electrochemical stability performance. In addition, the EIS assessment was conducted before and after performing 10,000 continuous GCD cycles and discussed in the supporting information.

Additionally, the high-performance SCp device has demonstrated feasibility and effectiveness in real-time applications by employing a coin-cell type configuration, as can be seen in Fig. 6. The fabrication of coin-cell SCp focuses on positive (NC(12)40-30) and negative (activated carbon) electrodes with aqueous electrolyte (6 M KOH) that are sealed with a coin-cell. In order to test real-time operation of electricity generation, two SCp coin-cells were wired in series with the "NC" terminal of eighteen 3 mm high-intensity light-emitting diodes (LEDs) (parallel connected). The three-digit LED voltmeter in the inset of Fig. 6(a) measures a maximum discharge voltage of 2.99 V after being charged with maximum SCp coin-cells voltage of 3 V, indicating an impressive performance of 99.67% achieved. The following four commercial LEDs that are typically used for "NC" LEDs illumination are red (~1.8 V), green (~2.3 V), blue (~2.6 V), and white (~2.8 V). This has been demonstrated by charging the coin-cells for 60 s and immediately lighting up LEDs as shown in Fig. 6(b-i). The LEDs flashed for a split of a second (Fig. 6(b-e)) before switching to their typical LED brightness (Fig. 6(f-i)) and lasted about 5 minutes. The power requirements for 18 LEDs can be calculated as 0.65 W, 0.83 W, 0.94 W, and 1 W for red (1.8V, 20mA), green (2.3V, 20mA), blue (2.6V, 20mA), and white (2.8 V, 20 mA), respectively. This illustrates the sudden discharge characteristics of capacitor-type behavior and long-time discharge attributes of battery-type behavior of the coin-cells. As a result, the nanoengineered *3D-on-2D* hierarchical structure of bimetallic LDH electrode provides an immense potential for a stable and reliable energy storage device for practical applications. The synergistic effect of *3D-on-2D* strategy can lead to the emergence of high conductivity, permeability, and faradaic active sites, which supports high active electrochemical capabilities to ensure efficient the charge transfer mechanism for high performance energy storage systems.

4. Conclusion

In summary, a 2D bimetallic NiCo LDH with 3D ZIF-67 nanoarchitecture on Ni foam battery-type electrode was fabricated in a two-step process using a simple low-cost strategy. The cathodic electrodeposition (CED) procedure was employed to achieve a 2D bimetallic NC(12)40 LDH, and 3D ZIF-67 hierarchical NC(12)40-30 electrode via pseudomorphic replication approach. The resulting maximum areal capacity of the *3D-on-2D* bimetallic NC(12)40-30 battery-type electrode is 1044 mC cm^{-2}, whereas the 2D bimetallic NC(12)40 LDH revealed is 661 mC cm^{-2} at a current density of 4 mA cm^{-2}. This suggests that the nanoengineered *3D-on-2D* bimetallic battery-type electrode endorses with higher electroactive sites with an outstanding reversible response of electrochemical kinetics, high reliability, and durability. Such hierarchical *3D-on-2D* structural functionalized battery-type electrode constitutes a promising candidate for energy storage systems due to the benefits of interfacial layer, higher density of electro active sites, rapid ion mobility, and enhanced redox behavior.

Acknowledgements

This research was supported by Basic Science Research Program through the National Research Foundation of Korea (NRF) funded by the Ministry of Education (NRF-2014R1A6A1030419) and by the National Research Foundation of Korea (NRF) Grant funded by the Korean government (MSIT) (No. 2020112382). This work has been partially supported by the Spanish government under project PID2019-109215RB-C41 (SCALED).

Conflict of Interest

The authors declare no conflict of interest.

References

[1] H. Zhou, H. Li, L. Li, T. Liu, G. Chen, Y. Zhu, L. Zhou, H. Huang, Structural composite energy storage devices — a review, Mater. Today Energy. 24 (2022) 100924. https://doi.org/https://doi.org/10.1016/j.mtener.2021.100924.

[2] H. Liu, X. Liu, S. Wang, H.-K. Liu, L. Li, Transition metal based battery-type electrodes in hybrid supercapacitors: A review, Energy Storage Mater. 28 (2020) 122–145. https://doi.org/https://doi.org/10.1016/j.ensm.2020.03.003.

[3] X. Wu, H. Yang, M. Yu, J. Liu, S. Li, Design principles of high-voltage aqueous supercapacitors, Mater. Today Energy. 21 (2021) 100739. https://doi.org/https://doi.org/10.1016/j.mtener.2021.100739.

[4] C.J. Raj, R. Manikandan, K.H. Yu, G. Nagaraju, M.-S. Park, D.-W. Kim, S.Y. Park, B.C. Kim, Engineering thermally activated NiMoO4 nanoflowers and biowaste derived activated carbon-based electrodes for high-performance supercapatteries, Inorg. Chem. Front. 7 (2020) 369–384. https://doi.org/10.1039/C9QI01085H.

[5] M.Z. Iqbal, U. Aziz, Supercapattery: Merging of battery-supercapacitor electrodes for hybrid energy storage devices, J. Energy Storage. 46 (2022) 103823. https://doi.org/https://doi.org/10.1016/j.est.2021.103823.

[6] L. Miao, Z. Song, D. Zhu, L. Li, L. Gan, M. Liu, Recent advances in carbon-based supercapacitors, Mater. Adv. 1 (2020) 945–966. https://doi.org/10.1039/D0MA00384K.

[7] W. Wei, Z. Chen, Y. Zhang, J. Chen, L. Wan, C. Du, M. Xie, X. Guo, Full-faradaic-active nitrogen species doping enables high-energy-density carbon-based supercapacitor, J. Energy Chem. 48 (2020) 277–284. https://doi.org/https://doi.org/10.1016/j.jechem.2020.02.011.

[8] X. Long, Z. Wang, S. Xiao, Y. An, S. Yang, Transition metal based layered double

hydroxides tailored for energy conversion and storage, Mater. Today. 19 (2016) 213–226. https://doi.org/https://doi.org/10.1016/j.mattod.2015.10.006.

[9] X. Luo, M. Zhong, P. He, J. Shao, Q. Wang, K. Li, W. Zhao, Transformation of 2D Co-LDH into 3D hierarchical hollow Co3O4 polyhedral arrays with enhanced electrochemical performance for supercapacitors, J. Alloys Compd. 826 (2020) 154241. https://doi.org/https://doi.org/10.1016/j.jallcom.2020.154241.

[10] L.D. Silva Neto, A.F. Silva, J.T. Freire, L. Meili, Chapter 11 - Fundamentals of layered double hydroxides and environmental applications, in: D. Giannakoudakis, L. Meili, I.B.T.-A.M. for S.E.R. Anastopoulos (Eds.), Elsevier, 2022: pp. 301–323. https://doi.org/https://doi.org/10.1016/B978-0-323-90485-8.00016-3.

[11] L. Mao, X. Zhao, Y. Li, L. Chen, New nickel-rich ternary carbonate hydroxide two-dimensional porous sheets for high-performance aqueous asymmetric supercapattery, J. Colloid Interface Sci. 624 (2022) 482–493. https://doi.org/https://doi.org/10.1016/j.jcis.2022.05.148.

[12] F. Liao, G. Yang, Q. Cheng, L. Mao, X. Zhao, L. Chen, Rational design and facile synthesis of Ni-Co-Fe ternary LDH porous sheets for high-performance aqueous asymmetric supercapacitor, Electrochim. Acta. 428 (2022) 140939. https://doi.org/https://doi.org/10.1016/j.electacta.2022.140939.

[13] X. Wang, H. Song, S. Ma, M. Li, G. He, M. Xie, X. Guo, Template ion-exchange synthesis of Co-Ni composite hydroxides nanosheets for supercapacitor with unprecedented rate capability, Chem. Eng. J. 432 (2022) 134319. https://doi.org/https://doi.org/10.1016/j.cej.2021.134319.

[14] T. Liu, J. Ding, Z. Su, G. Wei, Porous two-dimensional materials for energy applications: Innovations and challenges, Mater. Today Energy. 6 (2017) 79–95. https://doi.org/https://doi.org/10.1016/j.mtener.2017.08.006.

[15] H. Tan, Y. Zhou, S.-Z. Qiao, H.J. Fan, Metal organic framework (MOF) in aqueous energy devices, Mater. Today. 48 (2021) 270–284. https://doi.org/https://doi.org/10.1016/j.mattod.2021.03.011.

[16] H. Tan, Z. Liu, D. Chao, P. Hao, D. Jia, Y. Sang, H. Liu, H.J. Fan, Partial Nitridation-Induced Electrochemistry Enhancement of Ternary Oxide Nanosheets for Fiber Energy Storage Device, Adv. Energy Mater. 8 (2018) 1800685. https://doi.org/https://doi.org/10.1002/aenm.201800685.

[17] Z. Chen, Y. Ha, H. Jia, X. Yan, M. Chen, M. Liu, R. Wu, Oriented Transformation of Co-LDH into 2D/3D ZIF-67 to Achieve Co–N–C Hybrids for Efficient Overall Water Splitting, Adv. Energy Mater. 9 (2019) 1803918. https://doi.org/https://doi.org/10.1002/aenm.201803918.

[18] G.H.A. Therese, P.V. Kamath, Electrochemical Synthesis of Metal Oxides and Hydroxides, Chem. Mater. 12 (2000) 1195–1204. https://doi.org/10.1021/cm990447a.

[19] M. Wohlfahrt-Mehrens, R. Oesten, P. Wilde, R.A. Huggins, The mechanism of electrodeposition and operation of Ni(OH)2 layers, Solid State Ionics. 86–88 (1996) 841–847. https://doi.org/https://doi.org/10.1016/0167-2738(96)00192-0.

[20] T. Nguyen, M. Boudard, M.J. Carmezim, M.F. Montemor, Layered Ni(OH)2-Co(OH)2 films prepared by electrodeposition as charge storage electrodes for hybrid supercapacitors, Sci. Rep. 7 (2017) 39980. https://doi.org/10.1038/srep39980.

[21] C.-C. Hu, J.-C. Chen, K.-H. Chang, Cathodic deposition of Ni(OH)2 and Co(OH)2 for asymmetric supercapacitors: Importance of the electrochemical reversibility of redox couples, J. Power Sources. 221 (2013) 128–133. https://doi.org/https://doi.org/10.1016/j.jpowsour.2012.07.111.

[22] J. Reboul, S. Furukawa, N. Horike, M. Tsotsalas, K. Hirai, H. Uehara, M. Kondo, N. Louvain, O. Sakata, S. Kitagawa, Mesoscopic architectures of porous coordination

polymers fabricated by pseudomorphic replication, Nat. Mater. 11 (2012) 717–723. https://doi.org/10.1038/nmat3359.

[23] L. Shao, F. Fan, X. Dai, H. Fu, W. Li, W. Qi, F.-B. Meng, Y. Fu, Pseudomorphic Replacement in the Transformation between Metal–Organic Frameworks toward Three-Dimensional Hierarchical Nanostructures, Chem. Mater. 34 (2022) 5356–5365. https://doi.org/10.1021/acs.chemmater.2c00021.

[24] W. Sun, X. Zhai, L. Zhao, Synthesis of ZIF-8 and ZIF-67 nanocrystals with well-controllable size distribution through reverse microemulsions, Chem. Eng. J. 289 (2016) 59–64. https://doi.org/https://doi.org/10.1016/j.cej.2015.12.076.

[25] R. Wagia, I. Strashnov, M.W. Anderson, M.P. Attfield, Insight and Control of the Crystal Growth of Zeolitic Imidazolate Framework ZIF-67 by Atomic Force Microscopy and Mass Spectrometry, Cryst. Growth Des. 18 (2018) 695–700. https://doi.org/10.1021/acs.cgd.7b01058.

[26] K.M. Amin, K. Krois, F. Muench, B.J.M. Etzold, W. Ensinger, Hierarchical pipe cactus-like Ni/NiCo-LDH core–shell nanotube networks as a self-supported battery-type electrode for supercapacitors with high volumetric energy density, J. Mater. Chem. A. 10 (2022) 12473–12488. https://doi.org/10.1039/D2TA00235C.

[27] J.T. Mefford, A.R. Akbashev, L. Zhang, W.C. Chueh, Electrochemical Reactivity of Faceted β-Co(OH)2 Single Crystal Platelet Particles in Alkaline Electrolytes, J. Phys. Chem. C. 123 (2019) 18783–18794. https://doi.org/10.1021/acs.jpcc.9b03589.

[28] X. Guo, T. Xing, Y. Lou, J. Chen, Controlling ZIF-67 crystals formation through various cobalt sources in aqueous solution, J. Solid State Chem. 235 (2016) 107–112. https://doi.org/https://doi.org/10.1016/j.jssc.2015.12.021.

[29] R. Velayutham, R. Manikandan, C. Justin Raj, A. Dennyson Savariraj, W.-J. Cho, H.-M. Jang, B. Chul Kim, Rationally designed metal–organic framework templated iron-

molybdenum sulfide for high energy density hybrid supercapacitors, Appl. Surf. Sci. 570 (2021) 151051. https://doi.org/https://doi.org/10.1016/j.apsusc.2021.151051.

[30] T. Wang, S. Zhang, X. Yan, M. Lyu, L. Wang, J. Bell, H. Wang, 2-Methylimidazole-Derived Ni–Co Layered Double Hydroxide Nanosheets as High Rate Capability and High Energy Density Storage Material in Hybrid Supercapacitors, ACS Appl. Mater. Interfaces. 9 (2017) 15510–15524. https://doi.org/10.1021/acsami.7b02987.

[31] R. Li, Z. Hu, X. Shao, P. Cheng, S. Li, W. Yu, W. Lin, D. Yuan, Large Scale Synthesis of NiCo Layered Double Hydroxides for Superior Asymmetric Electrochemical Capacitor, Sci. Rep. 6 (2016) 18737. https://doi.org/10.1038/srep18737.

[32] Y. Wang, Y. Song, Y. Xia, Electrochemical capacitors: mechanism, materials, systems, characterization and applications, Chem. Soc. Rev. 45 (2016) 5925–5950. https://doi.org/10.1039/C5CS00580A.

[33] T. Yang, J. Ye, S. Chen, S. Liao, H. Chen, L. Yang, X. Xu, F. Wang, Construction of nanowall-supported-nanorod nico ldh array electrode with high mass-loading on carbon cloth for high-performance asymmetric supercapacitors, Electrochim. Acta. 362 (2020) 137081. https://doi.org/https://doi.org/10.1016/j.electacta.2020.137081.

[34] G. Zhong, D. Liu, J. Zhang, The application of ZIF-67 and its derivatives: adsorption, separation, electrochemistry and catalysts, J. Mater. Chem. A. 6 (2018) 1887–1899. https://doi.org/10.1039/C7TA08268A.

[35] P.S. Jijoe, S.R. Yashas, H.P. Shivaraju, Fundamentals, synthesis, characterization and environmental applications of layered double hydroxides: a review, Environ. Chem. Lett. 19 (2021) 2643–2661. https://doi.org/10.1007/s10311-021-01200-3.

[36] X. Shang, H. Mei, Z. Li, C. Dong, Z. Wang, B. Xu, Improved ionic diffusion and interfacial charge/mass transfer of ZIF-67-derived Ni–Co-LDH electrodes with bare ZIF-residual for enhanced supercapacitor performance, New J. Chem. 45 (2021)

13979–13985. https://doi.org/10.1039/D1NJ02201F.

[37] C. Hobbs, S. Jaskaniec, E.K. McCarthy, C. Downing, K. Opelt, K. Güth, A. Shmeliov, M.C.D. Mourad, K. Mandel, V. Nicolosi, Structural transformation of layered double hydroxides: an in situ TEM analysis, Npj 2D Mater. Appl. 2 (2018) 4. https://doi.org/10.1038/s41699-018-0048-4.

[38] W. Guo, C. Dun, C. Yu, X. Song, F. Yang, W. Kuang, Y. Xie, S. Li, Z. Wang, J. Yu, G. Fu, J. Guo, M.A. Marcus, J.J. Urban, Q. Zhang, J. Qiu, Mismatching integration-enabled strains and defects engineering in LDH microstructure for high-rate and long-life charge storage, Nat. Commun. 13 (2022) 1409. https://doi.org/10.1038/s41467-022-28918-0.

[39] L. Meng, B. Yu, Y. Qin, Templated interfacial synthesis of metal-organic framework (MOF) nano- and micro-structures with precisely controlled shapes and sizes, Commun. Chem. 4 (2021) 82. https://doi.org/10.1038/s42004-021-00522-1.

[40] X. Yi, H. Sun, N. Robertson, C. Kirk, Nanoflower Ni(OH)2 grown in situ on Ni foam for high-performance supercapacitor electrode materials, Sustain. Energy Fuels. 5 (2021) 5236–5246. https://doi.org/10.1039/D1SE01036K.

[41] A.M. Kale, R. Manikandan, C.J. Raj, R. Velayutham, W.-J. Cho, B.C. Kim, Post synthetic annealing of zeolitic imidazolate framework-67 for high-performance hybrid supercapacitors, Appl. Surf. Sci. 542 (2021) 148716. https://doi.org/https://doi.org/10.1016/j.apsusc.2020.148716.

[42] A.M. Kale, R. Manikandan, C. Justin Raj, A. Dennyson Savariraj, C. Voz, B.C. Kim, Protonated nickel 2-methylimidazole framework as an advanced electrode material for high-performance hybrid supercapacitor, Mater. Today Energy. 21 (2021) 100736. https://doi.org/https://doi.org/10.1016/j.mtener.2021.100736.

[43] A.D. Savariraj, R. Manikandan, C.J. Raj, R. Velayutham, R. V Mangalaraja, J. Park,

W.-J. Cho, B.C. Kim, Epitaxial Engineering Strategy to Amplify Localized Surface Plasmon Resonance and Electrocatalytic Activity Enhancement in Layered Bismuth Selenide by Phosphorus Functionalization, Batter. Supercaps. 5 (2022) e202100310. https://doi.org/https://doi.org/10.1002/batt.202100310.

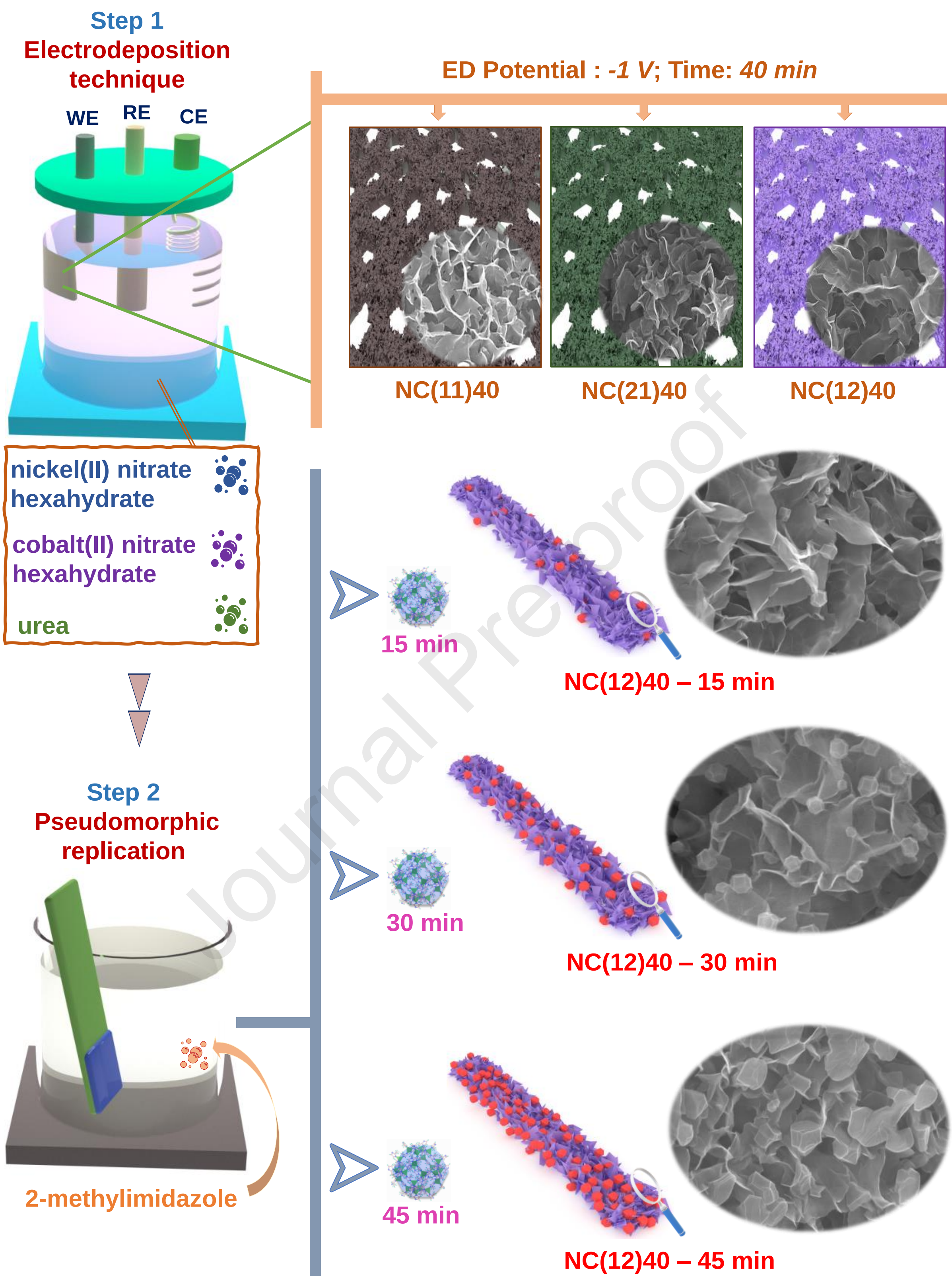

Fig. 1. Schematic illustration of the two-step fabrication of nanoengineered *3D-on-2D* hierarchical battery-type NiCo electrodes.

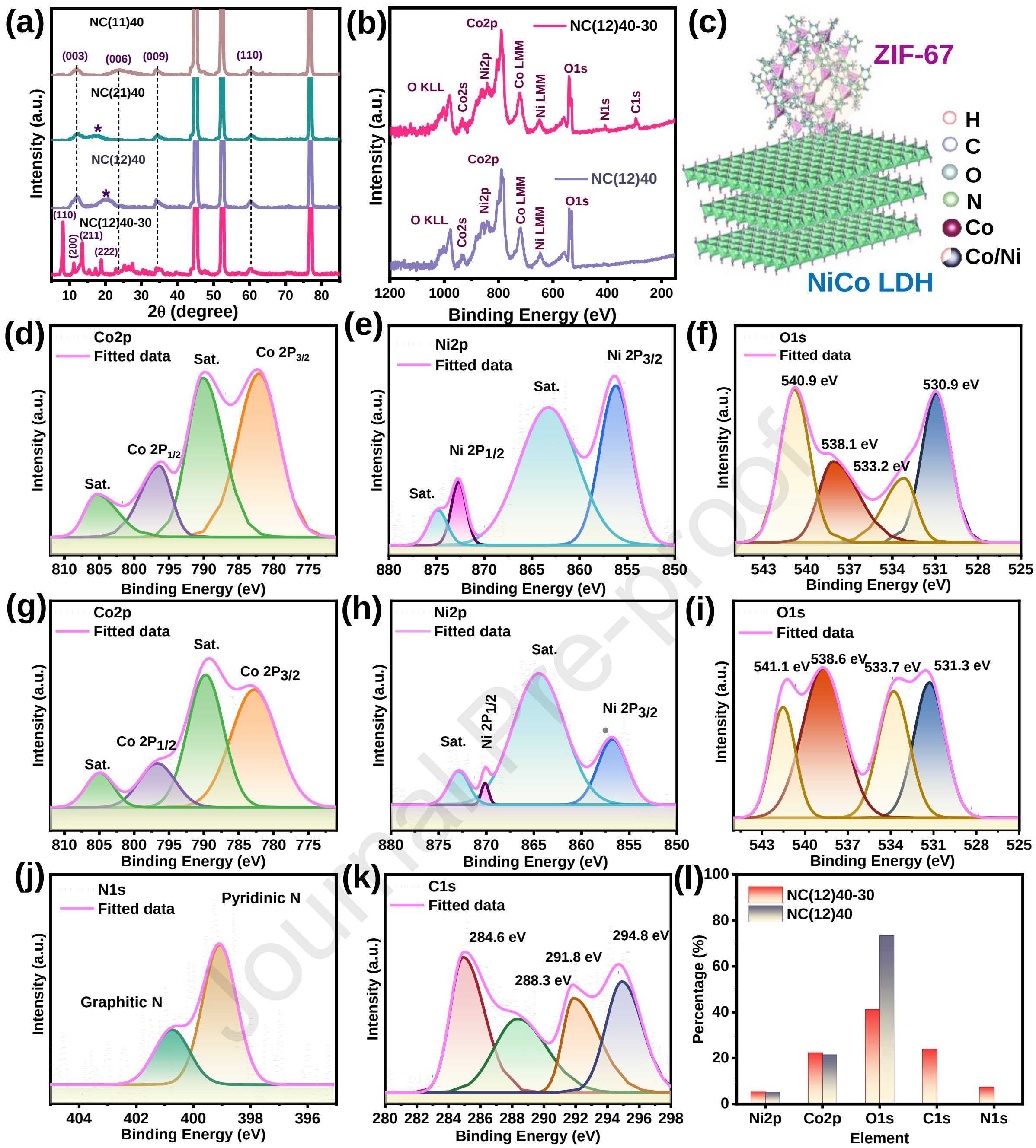

Fig. 2. Chemical composition characterization. (a) XRD patterns of *3D-on-2D* hierarchical of bimetallic LDH electrodes, (b) XPS survey spectra, (c) crystal structure of 2D NiCo LDH and 3D ZIF-67, (d-f) high resolution XPS spectra of NC(12)40 at (d) cobalt region (Co2p), (e) nickel region (Ni2p), (f) oxygen region (O1s), (g-k) high resolution XPS spectra of NC(12)40-30 at (g) cobalt region (Co2p), (h) nickel region (Ni2p), (i) oxygen region (O1s), (j) nitrogen region (N1s), (k) carbon region (C1s) and (l) XPS elemental composition of NC(12)40 and NC(12)40-30.

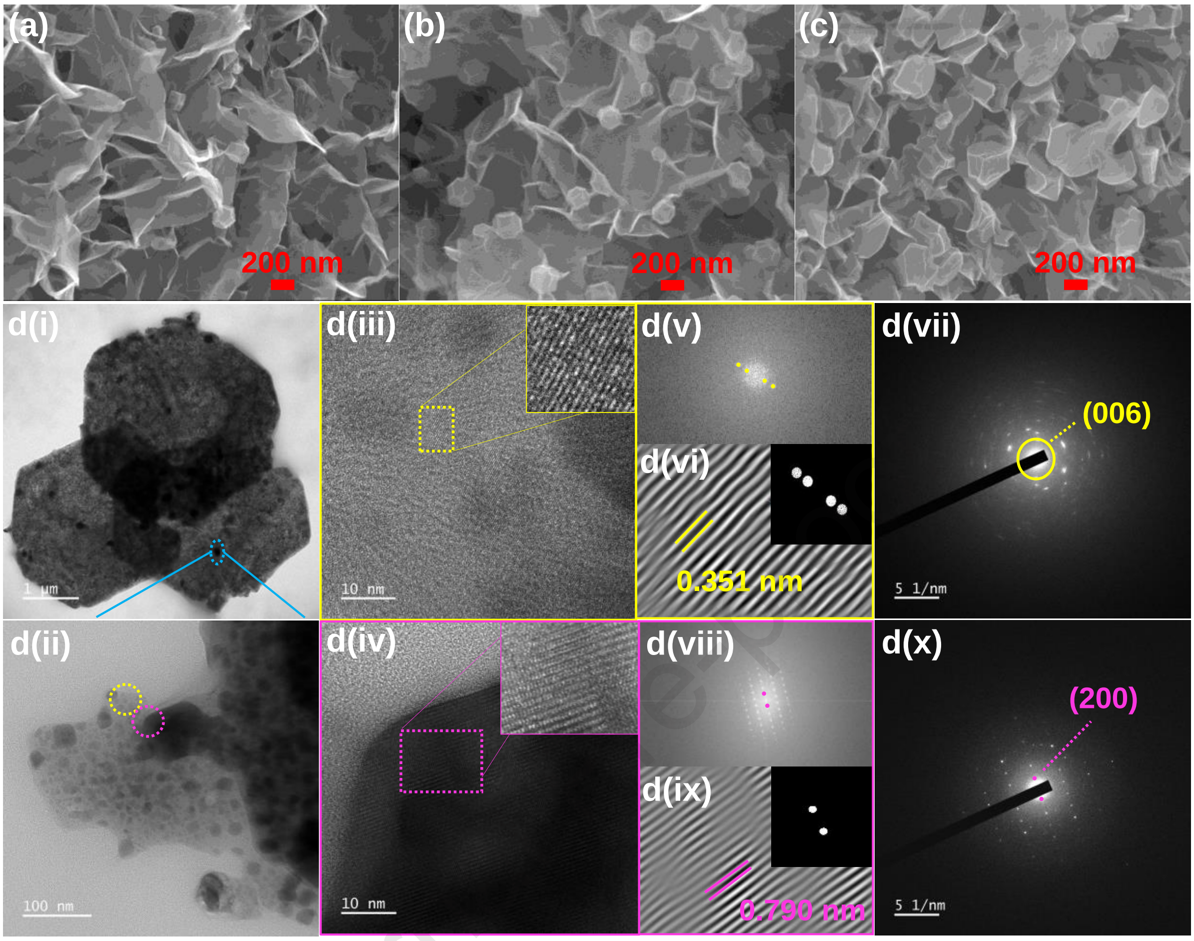

Fig. 3. Morphological analysis of *3D-on-2D* structural electrodes. The FE-SEM images of (a) NC(12)40-15, (b) NC(12)40-30 and (c) NC(12)40-45. HR-TEM micrograph analysis of NC(12)40-30 electrode using GMS software of (d)(i) magnifications of TEM images, (d)(ii-iv) selected sites of HR-TEM micrographs, (d)(v-vii) yellow selected HR-TEM micrograph of FFT, IFFT, and SAED pattern, and (d)(viii-x) pink selected HR-TEM micrograph of FFT, IFFT, and SAED pattern.

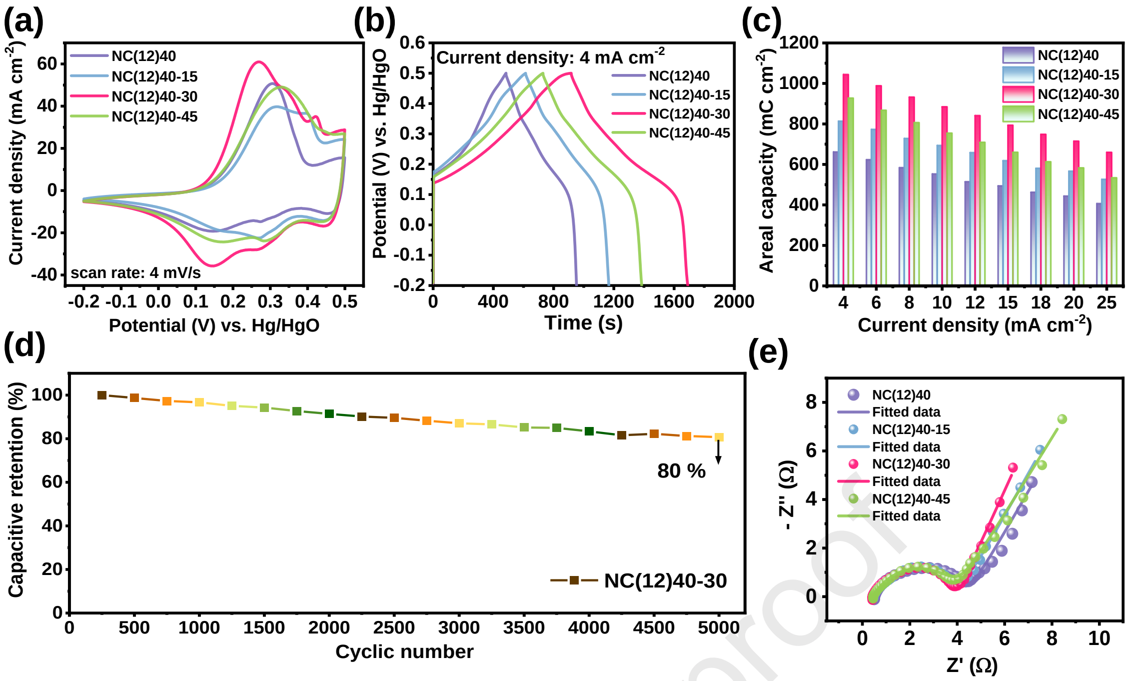

Fig. 4. Electrochemistry of *3D-on-2D* hierarchical bimetallic electrodes. (a) relative CVs curves, (b) comparative GCD profiles, and (c) areal capacity at various current densities, (d) cycling performances of NC(12)40-30 for 5,000 cycles at 15 mA cm^{-2}, and (i) Nyquist plots in the frequency range of 10 mHz to 100 kHz of *3D-on-2D* electrodes.

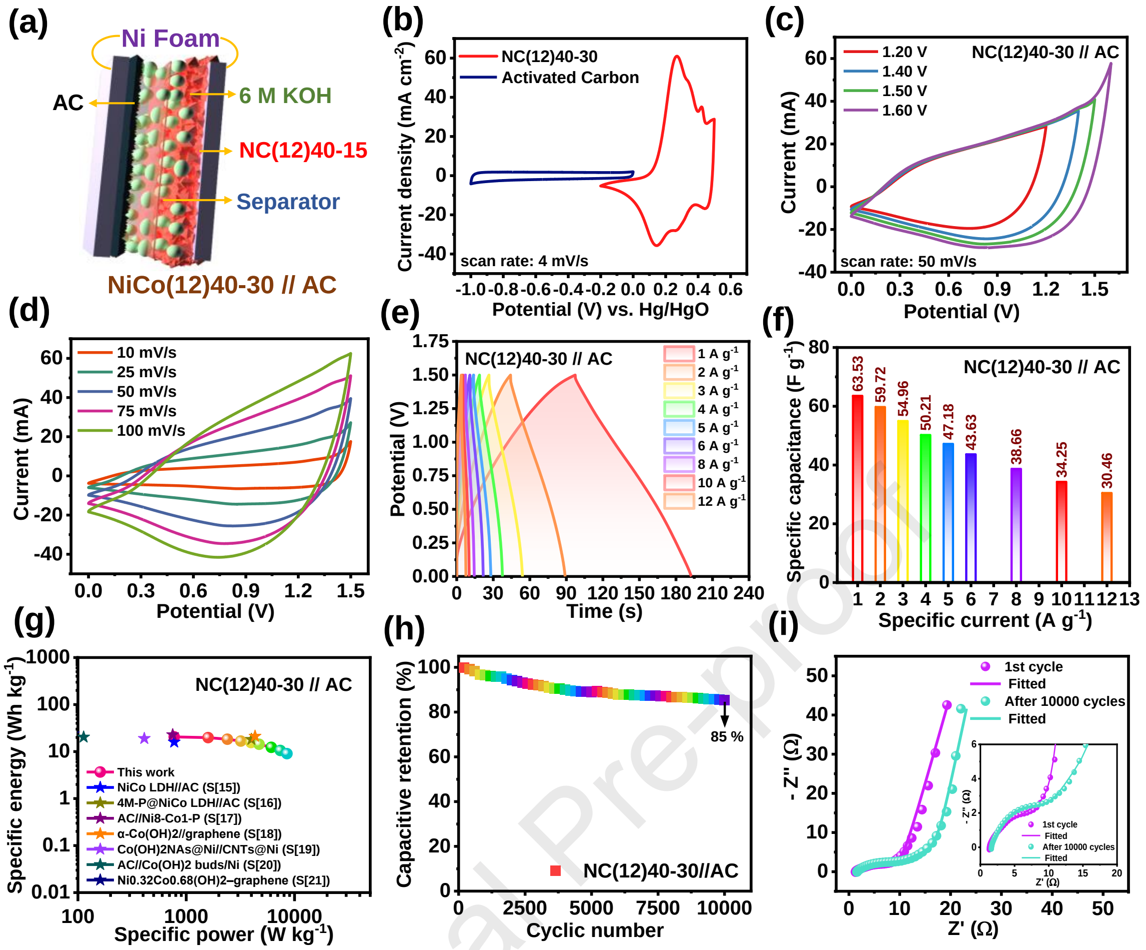

Fig. 5. Electrochemical performance of supercapattery device. (a) schematic illustration of a SCp device, (b) relative CVs of NC(12)40-30 and AC, and SCp device (NC(12)40-30//AC) analysis of (c) CVs of different voltage window, (d) different CVs scan rates, (e) various GCD specific currents, (f) specific capacitance, (g) Ragone plot, (h) long-life cycling performances for 10,000 charge/discharge cycles at 6 A g^{-1}, and (i) Nyquist plots of NC(12)40-30//AC determined before and after 10,000 cycles.

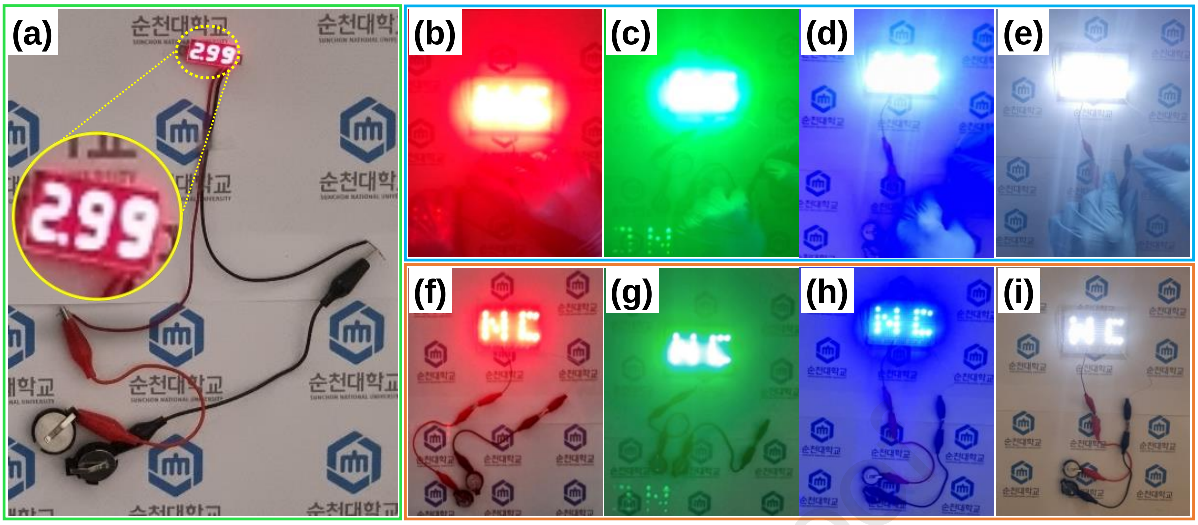

Fig. 6. Digital images of two series connected supercapattery coin-cell with, (a) three-digit LED voltmeter with inset magnification after charged, and (b-e) flash-like illumination of four commercial LEDs (red, green, blue, and white), and (f-i) typical LED brightness after about three seconds of flash-like illumination.

Highlights

- Nanoengineered *3D-on-2D* structured battery-type electrodes were fabricated using simple two-step platforms.
- Hierarchical 2D NiCo bimetallic LDH electrodes were achieved by cathodic electrodeposition techniques.
- Nanoengineered 3D ZIF-67 sodalite framework on the 2D LDH surface was attained via a pseudomorphic replication approach and reveals a maximum areal capacity of 1044 mC cm^{-2}.
- Assembled SCp coin cell displays 18-LED illumination in four different commercial LED colors for viability of supercapatteries.

Declaration of interests

☒ The authors declare that they have no known competing financial interests or personal relationships that could have appeared to influence the work reported in this paper.

☐ The authors declare the following financial interests/personal relationships which may be considered as potential competing interests: